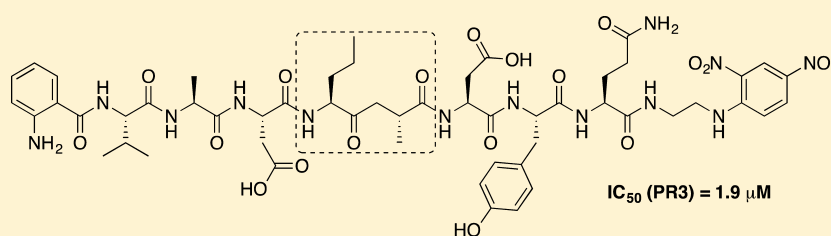


Reversible Ketomethylene-Based Inhibitors of Human Neutrophil Proteinase 3

Adnan Budnjo,^{†,#} Shailesh Narawane,^{‡,#} Cédric Grauffel,^{‡,§,-} Anne-Sophie Schillinger,^{‡,§} Torgils Fossen,[†] Nathalie Reuter,^{*,‡,§} and Bengt Erik Haug^{*,†}[†]Department of Chemistry and Centre for Pharmacy, University of Bergen, Allégaten 41, 5007 Bergen, Norway[‡]Department of Molecular Biology, University of Bergen, 5008 Bergen, Norway[§]Computational Biology Unit, University of Bergen, 5008 Bergen, Norway

S Supporting Information



ABSTRACT: Neutrophil serine proteases, proteinase 3 (PR3) and human neutrophil elastase (HNE), are considered as targets for chronic inflammatory diseases. Despite sharing high sequence similarity, the two enzymes have different substrate specificities and functions. While a plethora of HNE inhibitors exist, PR3 specific inhibitors are still in their infancy. We have designed ketomethylene-based inhibitors for PR3 that show low micromolar IC₅₀ values. Their synthesis was made possible by amending a previously reported synthesis of ketomethylene dipeptide isosteres to allow for the preparation of derivatives suitable for solid phase peptide synthesis. The best inhibitor (Abz-VADnV[Ψ](COCH₂)ADYQ-EDDnp) was found to be selective for PR3 over HNE and to display a competitive and reversible inhibition mechanism. Molecular dynamics simulations show that the interactions between enzyme and ketomethylene-containing inhibitors are similar to those with the corresponding substrates. We also confirm that N- and C-terminal FRET groups are important for securing high inhibitory potency toward PR3.

INTRODUCTION

Neutrophils, the most abundant type of leukocytes, are able to mediate both anti-infectious and pro-inflammatory effects and are key components of the innate immune system.^{1,2} Neutrophil serine proteases (NSPs) proteinase 3 (PR3, EC 3.4.21.76) and human neutrophil elastase (HNE) are homologous antimicrobial serine proteases of the polymorphonuclear neutrophils (PMNs). They are also key regulators of the inflammatory response³ and are considered as important cellular targets in a number of chronic inflammatory diseases.⁴ HNE and PR3 can be released extracellularly at sites of inflammation where they play a crucial role in the pathogenesis by degrading elastin and other matrix proteins causing tissue destruction that may lead to chronic obstructive pulmonary disease (COPD), cystic fibrosis, acute lung injury, and vasculitis.^{5–9} Antineutrophil cytoplasmic antibody (ANCA)-associated vasculitis is one such condition where PR3 acts as a specific autoantigen causing granulomatosis with polyangiitis (GPA).¹⁰ Unlike HNE, PR3 is only emerging as a target for these pathologies, and the lack of specific substrates and inhibitors for PR3 has certainly hindered investigations of its roles in the above-mentioned pathologies. Yet PR3 is proposed as a pharmacological target for therapeutic intervention in a

number of chronic inflammatory diseases,⁴ including GPA¹¹ and COPD.¹²

PR3 and HNE share a high sequence identity (56%) and structural similarity.¹³ They both adopt the typical fold of chymotrypsin-like serine proteases with one α -helix and two six-stranded β -barrels. Their active site is located between the two β -barrels and contains the catalytic triad consisting of histidine (His57), serine (Ser195), and aspartic acid (Asp102). The mechanism of peptide bond hydrolysis involves a nucleophilic attack by the Ser195 side chain hydroxyl group onto the carbonyl carbon of the scissile peptide bond, commonly denominated P1–P1' using the Schechter and Berger¹⁴ nomenclature.¹⁵ Interactions between the substrate and the extended ligand binding sites, also denominated using the same nomenclature, help to maintain the substrate in the active site. Although PR3 and HNE both preferentially cleave peptide bonds after small hydrophobic amino acids (at the P1 position), we have shown that they differ substantially in the nature of their S2, S1', S2', and S3' binding sites, leading to different enzyme–substrate interactions.^{13,16} Based on these differences, we and others have developed selective substrates

Received: May 8, 2014

for PR3 containing a negatively charged residue in P2 and P2' and positively charged residues in P1' and P3'.^{16,17} Highly selective substrates for PR3 that allow the detection of the protease in biological samples have also been developed.^{18,19} Most substrates are based on the fluorescence resonance energy transfer (FRET) principle, whereby the peptide contains N- and C-terminal fluorophore and quencher pairs that after hydrolysis of the peptide allow for selective detection of the fluorogenic hydrolysis product. For PR3 and HNE, N-terminal 2-aminobenzoic acid (Abz) and C-terminal *N*-(2,4-dinitrophenyl)-ethylenediamine (EDDnp) are among several commonly used fluorophores and quenchers, respectively (see Figure 1).^{20,21} We have recently shown that Abz-VADnVA-

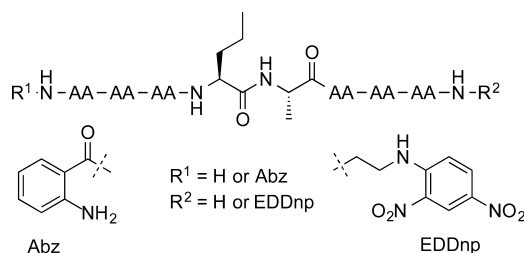


Figure 1. Substrates for PR3.

DYQ-EDDnp (nV = norvaline), which is reported to be highly selective for PR3,^{17,22} is more efficiently hydrolyzed at the nVal-Ala amide bond by PR3 than the corresponding peptides with an unmodified N-terminal amine and a C-terminal amide.²³ Using molecular dynamics simulations, we were able to explain the improvement of enzymatic efficiency by showing that the two fluorophores engage in interactions with the enzyme. In a recent study, Lesner and co-workers have prepared combinatorial libraries of PR3 substrates based on the sequence Abz-YY-Abu-X1'X2'X3'-Tyr(3-NO₂)-NH₂ (Abu = (2*S*)-aminobutyric acid), which enabled the discovery of Abz-YY-Abu-NEP-Tyr(3-NO₂)-NH₂ as a novel and highly specific PR3 substrate.²⁴

Because of the early identification of HNE as a drug target in, for example, COPD, numerous studies have been devoted to the development of HNE inhibitors. A recent report on the development of HNE substrates encompassing unnatural amino acids using a hybrid combinatorial substrate library approach, which also enabled the development of sensitive activity-based probes for HNE, may also lead to future development of new inhibitors.²⁵ Inhibitors reported include mechanism-based inhibitors, acylating agents targeting the active site serine, transition state analogues, and noncovalent inhibitors (see Groutas et al.⁵ for a review). Unlike for HNE,^{9,26–31} PR3 selective inhibitors are still in their infancy. Small molecule inhibitors have been reported,^{32–34} but no PR3 selective inhibitor is available, except for a recently reported azapeptide inhibitor.³⁵ This inhibitor, which is selective for PR3 and in which the α -carbon atom of a substrate P1 residue has been replaced by a nitrogen atom, acts as a noncovalent reversible inhibitor because it does not form an acyl-enzyme complex.³⁵

We here report a study on peptidomimetic PR3 inhibitors in which the scissile amide bond has been replaced with a noncleavable and electrophilic ketomethylene dipeptide isostere. Upon nucleophilic attack on the ketone by the active site serine, a tetrahedral hemiacetal will be formed. The hemiacetal will not be further cleaved, and its formation may in principle

lead to irreversible inhibition of the protease, or more likely it may exist in equilibrium with the ketone and alcohol thus acting through a covalent and reversible inhibition mechanism. The amino acid side chains on either side of the ketomethylene moiety may still form binding interactions with the protease binding pockets, thus securing the selectivity observed for the corresponding substrate sequence,³⁶ while formation of the covalent bond can increase the inhibitory potency.^{37,38} Having earlier developed PR3 selective substrates, we naturally thought of using the same sequences for peptidomimetics.

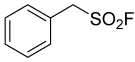
In the present study, we first verify using molecular docking and molecular dynamics simulations that the replacement of the scissile P1–P1' nVal–Ala amide bond by a ketomethylene moiety in the FRET substrates of our earlier study²³ does not perturb their positioning into the active site and interactions with the substrate binding sites. We further synthesize the peptidomimetic compounds, which were tested for their inhibitory activity against PR3 and HNE. We finally investigate the inhibition mechanism.

RESULTS AND DISCUSSION

The choice of peptidomimetic sequences is based on our earlier work on cleavable substrates where we varied (1) amino acids at positions P2, P2', and P3' in sequences of the type VA-P2-nVA-P2'P3'-Q and (2) the nature of the N- and C-terminal groups: either FRET groups Abz/EDDnp or H/NH₂. We named these substrates by the nature of their P2, P2', and P3' amino acids, as well as the presence or absence of a FRET group. For the ketomethylene compounds, we chose some of the most potent substrates we had identified, namely, D-DY_{FRET} (Abz-VADnVADYQ-EDDnp) and N-ER_{FRET} (Abz-VANnVAERQ-EDDnp), as well as their non-FRET equivalent D-DY (VADnVADYQ-NH₂) and N-ER (VANnVAERQ-NH₂). In addition, we evaluate the introduction of a serine residue at P2 yielding S-ER_{FRET} (Abz-VASnVAERQ-EDDnp). The sequences and names of the ketomethylene compounds are summarized in Table 1.

Molecular Modeling. Our simulations, started with the inhibitors positioned as the substrates were found to be,²³ indicate that this positioning is stable (See Figure 2). The RMSD on the backbone of the inhibitors ranges from 0.72 to 0.81 Å along the simulation time, which is comparable to backbone RMSD observed for PR3. We have collected

Table 1. List of Compounds

Compound	Sequence/structure
keto-D-DY	H-VADnV[Ψ](COCH ₂)ADYQ-NH ₂
keto-D-DY _{FRET}	Abz-VADnV[Ψ](COCH ₂)ADYQ-EDDnp
keto-N-ER	H-VANnV[Ψ](COCH ₂)AERQ-NH ₂
keto-N-ER _{FRET}	Abz-VANnV[Ψ](COCH ₂)AERQ-EDDnp
keto-S-ER _{FRET}	Abz-VASnV[Ψ](COCH ₂)AERQ-EDDnp
PMSF ^a	
A1PI ^b	α -1 Protease Inhibitor

^aPhenylmethanesulfonyl fluoride. ^b α 1-Protease inhibitor (A1PI) is a 52-kDa serpin also known as α 1-antitrypsin (A1AT).

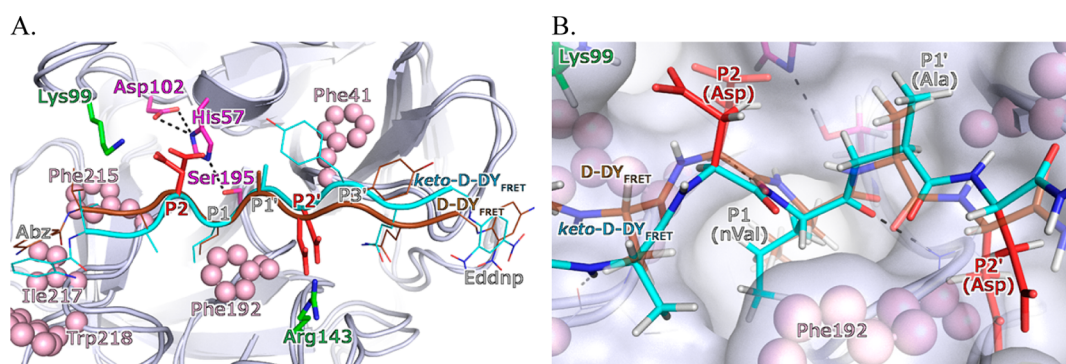


Figure 2. Predicted structure of substrate D-DY_{FRET} and peptidomimetic keto-D-DY_{FRET} bound to PR3. Structures after 2.5 ns long MD simulations: (A) active and binding sites and (B) zoom on P1–P1'. The protein is represented in gray cartoon, and the inhibitor and substrate backbones are represented in cyan and ochre, respectively. The catalytic triad (magenta), as well as the positively (green) and negatively (red) charged residues are shown with sticks, while residues predicted to mediate strong van der Waals interactions are represented with pink spheres.

distances and angles that characterize the geometry of the active site in Table 2. The distances between amino acids of the

Table 2. Geometry of PR3 Active Site from MD Simulations

atom names	data from	distance (Å)	angle (degrees)
N ^{e2} _{His57} –O ^g _{Ser195}	D-DY _{FRET}	2.9 ± 0.1	161 ± 10
	keto-D-DY _{FRET}	2.9 ± 0.1	161 ± 10
	keto-N-ER _{FRET}	2.9 ± 0.1	162 ± 9
O ^{d1} _{Asp102} –N ^{d1} _{His57}	D-DY _{FRET}	3.1 ± 0.3	144 ± 15
	keto-D-DY _{FRET}	3.1 ± 0.3	140 ± 15
	keto-N-ER _{FRET}	2.9 ± 0.2	150 ± 15
O ^{d2} _{Asp102} –N ^{d1} _{His57}	D-DY _{FRET}	3.1 ± 0.3	150 ± 15
	keto-D-DY _{FRET}	3.0 ± 0.3	153 ± 14
	keto-N-ER _{FRET}	3.1 ± 0.3	141 ± 16
O ^g _{Ser195} –C _{P1}	D-DY _{FRET}	3.2 ± 0.3	64 ± 9
	keto-D-DY _{FRET}	3.2 ± 0.2	62 ± 8
	keto-N-ER _{FRET}	3.1 ± 0.2	60 ± 8

catalytic triad reflect the presence of stable hydrogen bonds between Asp102 and His57 and between His57 and Ser195. The distances between the Ser195 nucleophilic oxygen and the P1 carbonyl carbon of the inhibitors are comparable to what we obtained from simulations of the enzyme complexed with cleavable peptides.

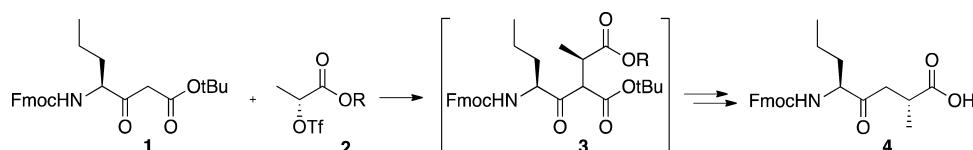
Further we conducted free energy decompositions on the trajectories to identify the strongest interactions stabilizing the PR3–inhibitor complexes. A detailed presentation of all contributions from both protein and peptidomimetics is given as Supporting Information (Figure S1) and reveals no difference between substrates and peptidomimetics that is higher than the uncertainty of the calculations. As can be expected from the conserved binding mode depicted in Figure 2, the pattern of interactions between the inhibitors and PR3 is similar to what was observed for the substrates. All peptidomimetics exhibit significant stabilization of their backbone in the P4–P1' segment, involving in particular several

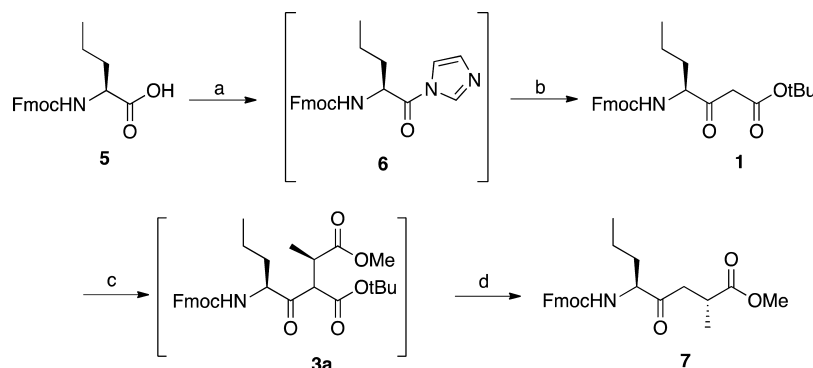
stable hydrogen bonds. The residues of this segment (and also Abz) are mediating strong van der Waals interactions, mainly with Phe192, Phe215, Ile217, and Trp218. The P1, nVal, is the amino acid with the strongest individual binding energy. Interactions of C-terminal residues are essentially mediated by the side chains, and it is obvious in both keto-D-DY_{FRET} and keto-N-ER_{FRET} that EDDnp and to a lesser extent the glutamine in P4' play an important stabilizing role (see Supporting Information).

Interactions between sites P2, P2', and P3' and charged residues Lys99, Arg143, and Asp61, respectively, are the ones that have been found able to confer selectivity for PR3 over HNE. Inhibitors keto-D-DY_{FRET} and keto-N-ER_{FRET} differ by the nature of P2 and P3'. We chose to keep a negatively charged residue in the P2' site because of the strong electrostatic interactions mediated with Arg143. Compared with a P2(Asp), a neutral asparagine mediates fewer hydrogen bonds with Lys99 (occupancy roughly divided by two, from 90% to 40%). The summed binding energy of these two partners is nevertheless similar in both compounds because the asparagine compensates with higher van der Waals interactions and is also able to form hydrogen bonds with the backbone of Ser214 (though to a moderate extent). Neutralizing the charge in P3' by going from arginine to tyrosine also reduces the hydrogen bond occupancy, though the Arg/Asp61 bond is not as stable as the other salt bridges (dwindling from 50% to 20%).

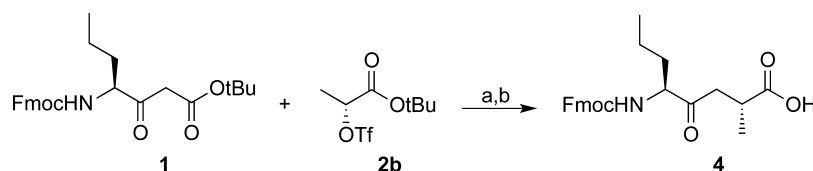
Because of the absence of high-resolution experimental data on the inhibitor–enzyme complexes, we had no other choice than initiating our simulations with the inhibitors already positioned in the ligand-binding sites, which is a reasonable choice for peptidomimetics. In order to prevent any potential bias due to the starting structure, each enzyme–inhibitor complex underwent five independent 2.5 ns long simulations. In an earlier study,¹⁶ we have shown that 2 ns long simulations of low-affinity substrates in the HNE or PR3 active site would lead to an obvious weakening of all substrate–enzyme interactions and of the Ser195–His57 hydrogen bond. Since

Scheme 1. Synthetic Strategy towards Dipeptide Isostere 4



Scheme 2. Synthesis of the Methyl Ester of Ketomethylene Dipeptide Isostere^a

^aReagents and conditions: (a) CDI, THF; (b), lithium 1-(*tert*-butoxy)ethen-1-olate, THF, $-78\text{ }^{\circ}\text{C}$ (72%); (c) (i) NaH, THF, $-20\text{ }^{\circ}\text{C}$; (ii) **2a**, THF, $-20\text{ }^{\circ}\text{C}$ to r.t.; (d) TFA, CH_2Cl_2 (75% over two steps).

Scheme 3. Synthesis of the Free Acid Ketomethylene^a

^aReagents and conditions: (a) (i) NaH, THF, $-5\text{ }^{\circ}\text{C}$; (ii) **2b**, $-5\text{ }^{\circ}\text{C}$ to r.t.; (b) TFA, CH_2Cl_2 (34% over two steps).

we observe none of these in our simulations of the ketomethylene peptidomimetics, we are confident that the enzyme–inhibitor complexes are stable adducts.

The simulations thus predict that ketomethylene peptidomimetics keto-D-DY_{FRET} and keto-N-ER_{FRET} would form adducts with PR3 similar to the Michaelis complexes formed between PR3 and the corresponding peptides (D-DY_{FRET} and N-ER_{FRET}, respectively). This suggests that these two peptidomimetics can act as competitive inhibitors for PR3.

Chemistry. We envisioned that the desired nVal–Ala ketomethylene dipeptide isostere **4**, suitable for Fmoc-based SPPS, could be accessed through the chemistry developed by Hoffman (Scheme 1).^{39,40} This approach relies on alkylation of the enolate of β -keto ester **1** using triflate **2**, which is obtained from a D-lactic acid ester. The alkylation occurs with inversion of the configuration on the lactic acid derivative C-2 to give intermediate **3**. Subsequent acidolysis and decarboxylation of the ester group in the α -position to the ketone, followed by hydrolysis of the second ester should give the required Fmoc-protected ketomethylene carboxylic acid **4**.

In our pursuit of **4**, we decided to investigate use of different combinations of esters for **3**. Methyl (*R*)-lactate is inexpensive and available in high enantiomeric purity (96% ee), and its use to prepare **3a** (see Scheme 1, R = Me) invokes hydrolysis of the methyl ester in the final step to give **4**. It should however be noted that basic hydrolysis of esters of ketomethylene dipeptide isosteres can be hampered by epimerization at C-5. Methyl (*R*)-lactate could be converted to triflate **2a** (see Scheme 1, R = Me) in good yield by reaction with triflic anhydride using 2,6-lutidine as acid scavenger (see Experimental Section).

In our initial route to **4**, Fmoc-protected norvaline (**5**) was activated by reaction with 1,1'-carbonyldiimidazole (CDI) in THF to give intermediate **6** (Scheme 2), which was directly reacted with the lithium enolate of *tert*-butyl acetate to afford keto ester **1** in 72% yield. Next, keto ester **1** was deprotonated using sodium hydride in THF and the resulting enolate was

allowed to react with triflate **2a**. The intermediate tricarboxylic compound **3a** was purified by flash column chromatography and NMR analysis revealed that it was in essence a single diastereoisomer, which is consistent with what has previously been reported.⁴⁰

Deprotection of the *tert*-butyl ester and successive decarboxylation was facilitated by treatment with trifluoroacetic acid (TFA) in CH_2Cl_2 to give methyl ester **7** in 75% yield over the two steps. Initially, the alkylation of **1** was carried out using triflate dissolved in CH_2Cl_2 , as has previously been reported to work well;⁴⁰ however we could only obtain **7** in 28% yield under these conditions. To our dismay, all attempts at chemoselectively deprotecting the methyl ester of **7** applying AlCl_3 and *N,N*-dimethylaniline as described by Liguori and co-workers⁴¹ failed to give the desired carboxylic acid **4** (see Scheme 1) without epimerization occurring. Trimethyltin hydroxide has been reported to be a mild reagent for ester hydrolysis;⁴² however in our case reactions with 5–10 equiv of Me_3SnOH at $80\text{ }^{\circ}\text{C}$ in 1,2-dichloroethane gave a mixture of epimerized ester and epimerized carboxylic acid. Similar results have been reported by the Skrydstrup group for the attempted hydrolysis of a ketomethylene containing tripeptide methyl ester.⁴³ In our case, prolonged reaction time (up to 65 h) with Me_3SnOH also gave Fmoc-deprotection in combination with epimerization and partial methyl ester deprotection. It seems that in our case, C-5 is very sensitive to epimerization under the different conditions applied. It should be noted that loss of chirality has also been reported to occur upon the formation of the calcium salt of Boc-Ile[Ψ](COCH_2)Phe-OH,⁴⁴ and under the mild conditions of benzyl ester formation using Cs_2CO_3 and benzyl bromide in an effort toward protection of the aspartate side chain of an Asp–Gly ketomethylene dipeptide isostere.⁴⁵

Since our original approach failed, we investigated the use of the same ester group on both the keto ester and the triflate (Scheme 3), because this potentially could give the advantage

of deprotecting both esters and give decarboxylation in the same step. One caveat of this approach is that the required *tert*-butyl D-lactate is quite expensive, but fortunately, it could be converted to triflate **2b** in high yield (89%) by reaction with triflic anhydride and 2,6-lutidine in CH₂Cl₂ (see Experimental Section).

Alkylation of **1** using **2b** was carried out as described above using **2a**, and submission of the crude alkylation product to one-pot ester deprotection and decarboxylation gave the Fmoc-protected ketomethylene carboxylic acid **4** in 34% yield over two steps (four transformations). Doubling the amount of triflate **2b**, increasing the reaction temperature to 0 °C, or extending the alkylating reaction time to 24 h did not result in increased yield.

Next, we incorporated the ketomethylene building blocks into 8-mer peptide sequences that we have previously identified as efficient and selective substrates for PR3. Synthesis of the peptidomimetics (see Table 1 for sequences) was achieved using an Fmoc-based SPPS protocol. During the synthesis of the peptidomimetics, all Fmoc-deprotection steps were kept at a minimum (2 × 2 min treatment with a 20% piperidine solution in DMF with or without HOBt) to avoid any epimerization at C-5 of the ketomethylene dipeptide isostere.⁴⁴ HPLC analysis of the crude products revealed that little or no epimerization had occurred during SPPS. In order to minimize aspartimide formation for the aspartate and asparagine residues,^{46,47} Fmoc-deprotection following the incorporation of either of these residues into the peptides was carried out by adding 0.1 M HOBt in the piperidine solution.⁴⁶ Analysis of the relevant crude products by LC-MS indicated that aspartimide formation had occurred to some extent, which was evident by the presence of peaks in the crude product with a *m/z* corresponding to the loss of water. Aspartimides are often hydrolyzed during peptide workup and purification;^{46,47} however, purification of the crude products proved to be very difficult for the keto-peptides not containing the FRET groups. Particularly keto-D-DY was difficult to purify, and the material used for biological assay contains either a mixture of epimers or possibly a mixture of the α - and β -aspartyl isomers in addition to minor amounts of aspartimide. Because the non-FRET compounds showed no activity in the initial assay (see Figure 3 below), further attempts at purifying keto-D-DY were abandoned. In order to ensure that we had obtained the desired α -aspartyl keto-D-DY_{FRET} and not the side product containing the β -aspartyl residue analogs upon purification, full structural elucidation of the FRET group containing peptidomimetics (see Table 1) was carried out (see Supporting Information). For keto-N-ER_{FRET}, the MS and NMR analyses revealed that the desired asparagine-containing peptidomimetic had been isolated instead of the side product containing an α - or β -aspartyl residue that would have formed upon hydrolysis of the aspartimide. The NMR analysis of keto-D-DY_{FRET} revealed strong NOESY *H_{αi}/NH(i + 1)* crosspeaks between Asp3 and the ketomethylene dipeptide isostere, as well as between Asp5 and Tyr6, which confirms an α -peptide chain for both aspartate residues (see Supporting Information for full NMR signal assignment).

In addition to the Fmoc-protected ketomethylene dipeptide isostere **4**, we also prepared the Boc-protected analog **8** (Scheme 4). Conversion of D-alanine (**9**) to D-lactic acid (**10**) followed by benzylation of the corresponding cesium salt to give **11**, which was subsequently reacted with triflic anhydride as described above, gave triflate **2c**.

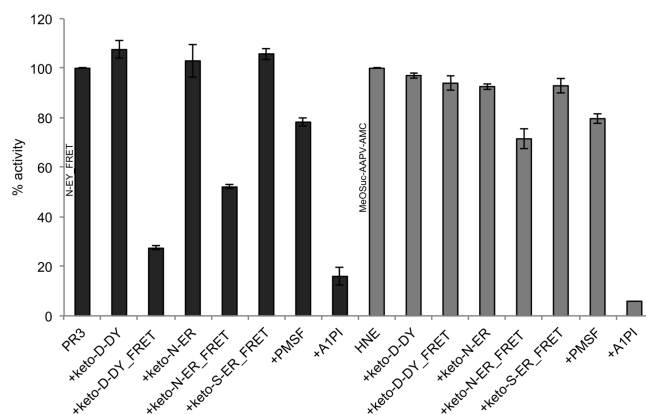
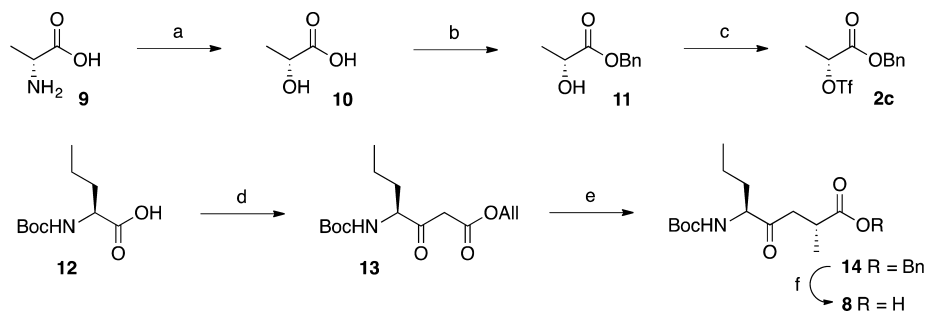


Figure 3. Effect of peptidomimetics and known inhibitors on the activity of purified PR3 and HNE. Activity of 0.5 nM purified PR3 and HNE in the presence of fixed concentration (6 μ M) of inhibitors on hydrolysis of FRET substrates Abz-VANnVAEYQ-EDDnp and MeOSuc-AAPV-AMC, respectively, after 30 min at 37 °C. The activity plotted is the relative activity in the presence of the inhibitor using as reference the activity in absence of any inhibitor. Error bars represent the standard error calculated from standard deviation of three independent experiments.

Next, Boc-protected norvaline (**12**) was activated with CDI and reacted with the lithium enolate of allyl acetate to afford keto ester **13** in 84% yield.⁴⁸ Alkylation of **13** using triflate **2c** followed by Pd(II) mediated cleavage of the allyl ester, which results in subsequent decarboxylation, gave benzyl ester **14** in 42% yield over the two steps and three transformations. Final hydrogenolysis of **14** gave carboxylic acid **8** in near quantitative yield. For the synthesis of keto-N-ER_{FRET}, both the Fmoc- and the Boc-protected ketomethylene dipeptide isostere were employed. Following coupling of the Boc-protected **8** onto the solid supported peptide, the Boc protecting group was removed using 4 M HCl in dioxane (see Experimental Section).⁴⁹ Prior to this, we had tested that the Pbf protecting group of Fmoc-Arg(Pbf)-OH was not cleaved under these conditions. The remainder of the peptide sequence was completed using the Fmoc protocol, and the crude peptide product was found by analytical HPLC analysis to be comparable to the one obtained using the Fmoc-protected isostere **4** (data not shown). The crude peptide yield following incorporation of Boc-protected **8** was however found to be lower (86% compared with 94% after incorporation of Fmoc-protected **4**), suggesting that partial cleavage of the incompletely assembled peptide from the Rink amide polymer support has occurred during the Boc-deprotection.

Biological Studies. Activity Assays. We tested the ability of each peptidomimetic to inhibit the hydrolysis of the substrates Abz-VANnVAEYQ-EDDnp (N-EY_{FRET}) by PR3 and MeOSuc-AAPV-AMC by HNE. We have earlier shown²³ that the former substrate was efficiently cleaved by PR3, while the latter has been used by Schepetkin et al. to conduct high throughput screening of compound libraries on HNE.⁵⁰

The activity of the enzymes incubated with each of the ketomethylenes is compared with their activity in the absence of the inhibitors, and we report the corresponding normalized activities in Figure 3. We also compare these with the activity of the proteases incubated with the endogenous inhibitor α -1 protease inhibitor (A1PI), as well as with a common synthetic serine protease inhibitor phenylmethanesulfonyl fluoride (PMSF).

Scheme 4. Synthesis of Boc-Protected Isostere **8^{cr}**

^aReagents and conditions: (a) NaNO₂, H₂O/TFA (62%); (b) (i) Cs₂CO₃, MeOH/H₂O; (ii) BnBr, DMF (75%); (c) Tf₂O, 2,6-lutidine, CH₂Cl₂, 0 °C (63%); (d) (i) CDI, THF; (ii) lithium 1-(allyloxy)ethen-1-olate, THF, -78 °C (84%); (e) (i) NaH, THF, -20 °C; (ii) **2c**, THF, -20 °C to rt; (iii) Pd(OAc)₂, PPh₃, HCO₂H, Et₃N, THF (42% over two steps); (f) 10% Pd/C, H₂, EtOH (quant.).

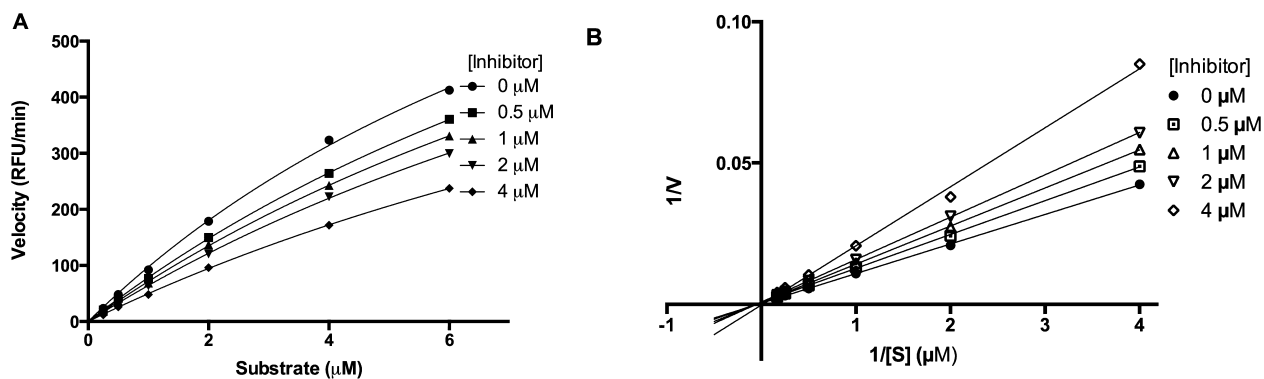


Figure 4. (A) Substrate titration (0–6 μM Abz-VADnVADYQ-EDDnp, D-DY_{FRET}) of steady-state velocity for PR3 (0.2 nM) in the presence of inhibitor keto-D-DY_{FRET} (0–4 μM). (B) Data from panel A plotted in double reciprocal form.

We observe selective inhibition of PR3 by compound keto-D-DY_{FRET} and compound keto-N-ER_{FRET}, although to a lesser extent for the latter. In agreement with earlier observations on the effect of FRET groups on substrate hydrolysis, the non-FRET counterparts of these peptidomimetics (i.e., compounds keto-D-DY and keto-N-ER) did not show any inhibitory activity. Compound keto-S-ER_{FRET}, a FRET peptidomimetic with a P2 serine, did show limited inhibition of HNE but not of PR3 in the assay conditions. The endogenous inhibitor A1PI was the most potent inhibitor for both enzymes, while PMSF showed up to 20% inhibition of PR3 and HNE.

Keto-D-DY_{FRET} Is a Competitive and Reversible Inhibitor. We performed a substrate titration of the steady-state velocity for PR3 in the presence of varying concentrations of keto-D-DY_{FRET}. Increasing the concentration of the inhibitor yields a reduction in the steady state velocity (Figure 4A), but not of the value of V_{max} which is evident from the double reciprocal plot of the same data (Figure 4B) that intersects at the y-axis indicating competitive inhibition.⁵¹ This is in agreement with the molecular dynamics simulations indicating that the peptidomimetics bind favorably to the substrate-binding site of the enzyme.

Next, we performed a rapid dilution assay in order to determine the reversibility of the inhibition by keto-D-DY_{FRET}. As can be seen from Figure 5, the protease activity could be fully recovered after rapid dilution of an inhibitor–protease solution into a solution of the substrate Abz-VADnVADYQ-EDDnp (D-DY_{FRET}); thus inhibition of PR3 by keto-D-DY_{FRET} is fully reversible.⁵¹

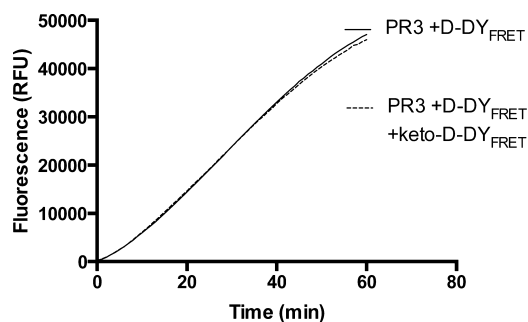
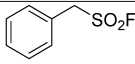


Figure 5. Rapid dilution experiment to determine the reversibility of inhibition by keto-D-DY_{FRET}. After 30 min incubation at room temperature, PR3 (50 nM) and keto-D-DY_{FRET} (19 μM) were rapidly diluted (100 times) into the reaction mixture containing 8 μM FRET substrate (Abz-VADnVADYQ-EDDnp) (dashed line); similarly PR3 alone was rapidly diluted in the reaction mixture containing the same FRET substrate (black line). The data presented is the mean of three experiments; error bars are not displayed for the sake of clarity (see Supporting Information, Figure S2).

Determination of IC₅₀. We further performed dose–response experiments on the two active inhibitors in order to determine their IC₅₀ values. To prevent bias due to intermolecular quenching between FRET substrates at high concentrations, we used a HPLC-based assay, instead of the fluorescent assay used above. The results are reported in Table 3. The two positive controls, PMSF and A1PI, were found to inhibit PR3 at concentrations comparable to what has been reported in the literature.⁵²

Table 3. Inhibitory Activity against PR3

Compound	Sequence	PR3 IC ₅₀ ^a	95% CI ^b
keto-D-DY _{FRET}	Abz-VADnV[Ψ](COCH ₂)ADYQ-EDDnp	1.91	1.87-1.95
		0.53 ^c	0.45-0.63 ^c
keto-N-ER _{FRET}	Abz-VANnV[Ψ](COCH ₂)AERQ-EDDnp	10.38	9.91-10.87
PMSF		19.23	16.46-22.51
α1PI	α-1 Protease Inhibitor	0.060	0.047-0.076

^aAbz-VADnVADYQ-EDDnp (D-DY_{FRET}) used as substrate. IC₅₀ values are given in μM. The values are obtained from fitting points that are the average of two independent experiments (see Experimental Section and Supporting Information for dose–response curves with error bars). ^b95% confidence intervals. ^cIC₅₀ for keto-D-DY_{FRET} determined using the N-ER_{FRET} substrate.

The inhibitor keto-D-DY_{FRET} showed the highest activity with an IC₅₀ value of 1.91 μM using the D-DY_{FRET} substrate. As the determination of the IC₅₀ was performed using HPLC data and because substrate and inhibitors are very similar, the fitting of the dose–response plot relies on fewer points than for the other inhibitors (Cf. Methods section and Supporting Information). Therefore, we also determined the IC₅₀ of keto-D-DY_{FRET} with a different substrate (N-ER_{FRET}) and find it to be equal to 0.5 μM. The keto-D-DY_{FRET} inhibitor is thus the most potent of our ketomethylenes. This is also consistent with our previously reported specificity constants (k_{cat}/K_m) for the parent substrates. Replacement of the negatively charged P2 aspartate with a polar uncharged asparagine by incorporation of the ketomethylene into the Abz-VANnVAERQ-EDDnp substrate slightly reduced the inhibitory activity (Table 3).

Since the assay is done at substrate concentrations significantly lower than the substrate's K_m (35.1 μM²³), and since the inhibitors are competitive, it is reasonable to estimate that the K_i for both inhibitors is close to their IC₅₀ values under equilibrium conditions.^{53,54} Knowing the concentration of the enzyme and the K_m of the substrate used for the dose–response experiment, we used the IC₅₀-to- K_i converter of the *BotDB* server⁵⁴ to predict K_i values for the two peptidomimetics. The server predicted K_i values of 1.7 and 9.1 μM for keto-D-DY_{FRET} and keto-N-ER_{FRET}, respectively. The value obtained for keto-D-DY_{FRET} is in the range of the one obtained for an azapeptide with a similar sequence³⁵ (Abz-VAD[aza]_nVADYQ-Y(NO₂), $K_i = 1.5$ μM).

CONCLUSIONS

We herein describe the synthesis of an Fmoc-protected nVal–Ala ketomethylene dipeptide isostere that has been incorporated into 8-mer peptide sequences in place of the nVal–Ala dipeptide using Fmoc-based SPPS. In the synthetic protocol for the ketomethylene dipeptide isostere, the use of *tert*-butyl ester protection for the carboxylic acid allows for its liberation without compromising the chiral integrity of the ketomethylene C-5.

Further, our activity assays show that incorporation of the ketomethylene dipeptide isostere into known substrates for PR3 yields peptidomimetic inhibitors with IC₅₀ values in the low micromolar range. The most potent PR3 inhibitors are Abz-VADnV[Ψ](COCH₂)ADYQ-EDDnp (keto-D-DY_{FRET}) and Abz-VANnV[Ψ](COCH₂)AERQ-EDDnp (keto-N-ER_{FRET}). While the former exclusively inhibits PR3 in our assay and can thus be regarded as highly selective for that

enzyme, the latter inhibits HNE as well although to a lesser extent than PR3. Furthermore, we estimate the K_i value of the keto-D-DY_{FRET} to be 1.7 μM, which is in agreement with the reported K_i value (1.5 μM) for an azapeptide-based inhibitor with a similar sequence.³⁵

Using molecular dynamics simulations, we verify that PR3 substrates and the corresponding ketomethylene-containing peptidomimetic inhibitors mediate comparable interactions with the ligand binding sites. We also show that the hydrogen bonds between amino acids of the catalytic triad and the position of the P1–P1' amino acids in the catalytic site are compatible with a nucleophilic attack of Ser195 onto the ketomethylene carbonyl group. In agreement with this, the substrate titration of the steady-state velocity for PR3 in the presence of keto-D-DY_{FRET} indicates a competitive inhibition, further strengthening the findings of the MD simulations. Thus, the inhibitors may very well bind to PR3 through the covalent bond formation of a hemiacetal,⁵⁵ and the reversibility assay indicates that the hemiacetal may exist in equilibrium with the ketone and alcohol.

We also show that the presence of the N-terminal Abz and C-terminal EDDnp FRET groups are required for inhibitory activity against PR3. In this respect, it is interesting to note that the only other peptidomimetic PR3 inhibitor published to date contains a N-terminal Abz and a C-terminal nitrotyrosine residue;³⁵ the latter is likely to be equivalent to EDDnp in its mode of interaction with PR3. We envision that peptidomimetic inhibitors without large hydrophobic groups in P5 and P'5 are likely to yield a lower inhibitory activity, unless one uses sequences that allow interactions at other binding sites to be stronger than those we observe.

Overall, the results presented provide important insight into further development of selective inhibitors for PR3, both for *in vitro* use and for the development of therapeutically relevant compounds.

EXPERIMENTAL SECTION

Molecular Modeling. We here use the same computational strategy as we used to design substrates for PR3 and HNE.²³ We perform five independent 2.5 ns long MD simulations for each of the keto-D-DY_{FRET} and the keto-N-ER_{FRET} inhibitors initially positioned in the PR3 active site. The simulations and their subsequent analyses serve two purposes: (i) to investigate the structure of the complexes and in particular the positioning of the peptidomimetics in the active site of PR3 and (ii) to evaluate the influence of the ketomethylene sequence on the interaction with the enzymes binding sites. The latter goal is achieved by analyzing trajectories using molecular mechanics/

Poisson–Boltzmann surface area (MM/PBSA) free energy decomposition.

Molecular Dynamics Simulations. We used the X-ray structure of PR3 (PDB ID 1FUJ) and the structure of PR3–peptide complexes, taken from our earlier simulations,²³ to position the ketomethylene peptidomimetics. The peptidic bond between the P1 and P1' amino acids was substituted by a ketomethylene group. In order to avoid bias in comparison, the whole protocol, encompassing system preparation, molecular dynamics (MD) simulations, and analysis, is the same as the one used for the substrates as previously described by our group.²³ All calculations were performed with the CHARMM force field (version 22⁵⁶ with CMAP correction⁵⁷). We used previously reported parameters²³ for the Abz and EDDnp groups, while the peptide bond dihedral parameters were modified for the P1–P1' link so as to reproduce a DFT/B3LYP/6-31G* torsion potential. The systems were first minimized with CHARMM⁵⁸ using harmonic restraints and then solvated in a cubic box of TIP3P water. Addition of two Cl[−] counterions was only required to neutralize the system with keto-N-ER_{FRET}. This was followed by a last energy minimization without restraints, and the systems were finally subjected to molecular dynamics simulations with NAMD.⁵⁹ The simulations were performed in the NPT ensemble at a temperature of 300 K, with an integration time step of 1 fs. These consisted of four successive heating phases (10, 100, 200, and 300 K), a 150 ps-long equilibration phase, and a production phase of 2.5 ns. In order to increase conformational sampling, five replicas, differing by the initial velocity distribution, were run for each system. The last 2 ns of the replicas are used for the analysis (which leads to an effective analysis window of 10 ns for each system).

Trajectory Analysis. The protocol used to obtain the energetic contributions of all amino acids to the formation of the complexes is based on the MM/PBSA approach.⁶⁰ Briefly, 25 representative conformations are extracted from each trajectory. van der Waals interactions and nonpolar contributions are evaluated with CHARMM⁵⁸ using Lennard-Jones potential and solvent accessible surface area analysis, respectively. Electrostatics is evaluated using the program UHBD.⁶¹ These decompositions are performed at the backbone/side chain level in order to get more insights into interactions. The criteria for hydrogen bonds are the following: acceptor (A) to hydrogen distance equal to or below 2.4 Å and angle D–H–A (D, hydrogen bond donor) equal to or greater than 130°. These two criteria must be met for at least 10 ps. The donor and acceptor definitions are from the CHARMM force field.⁵⁶

Chemistry. Chemicals and solvents were purchased from Sigma-Aldrich and used as delivered unless otherwise stated. Fmoc-Glu(EDDnp)-OH was prepared as described previously.²³ All moisture sensitive reactions were carried out under argon atmosphere in oven-dried equipment that was cooled under vacuum. Solvents used for moisture sensitive reactions were obtained from the Department of Chemistry anhydrous solvent delivery system (SPS-800 system from M. Braun GmbH, Garching, Germany) at the University of Bergen. Flash column chromatography was performed using silica gel from Merck (silica gel 60, 0.040–0.063 mm), supplied by VWR. TLC analyses were performed on aluminum sheets coated with Merck TLC silica gel 60 F₂₅₄ and visualization was achieved by using ultraviolet light (254 nm) or a solution of phosphomolybdic acid in ethanol. The NMR experiments were performed on a Bruker 400 MHz, a Bruker 500 MHz, or a Bruker 600 MHz with cryoprobe spectrometer at ambient temperature and with TMS as the internal standard, unless otherwise noted. All coupling constants are given in Hz. Positive and negative ion electrospray ionization mass spectrometry was conducted on either a Thermo electron LTQ Orbitrap XL spectrometer (Thermo, Bremen, Germany) or a JMS-T100LC AccuTOF spectrometer (JEOL, Inc. Peabody, MA, USA). Polarimetric measurements were done on an Optical Activity LTO AA-10R automatic polarimeter. The purity of tested compounds was assessed using RP HPLC (UV 220 nm).

tert-Butyl (S)-4-(((9H-Fluoren-9-yl)methoxy)carbonyl)amino)-3-oxoheptanoate (1). Fmoc-nVal-OH (5; 3.10 g, 9.15 mmol) was dissolved in dry THF (18 mL) under argon atmosphere, and CDI

(1.56 g, 9.60 mmol) was added to the solution under stirring. The reaction mixture was left under stirring for 1.5 h while LDA was prepared by dissolving diisopropylamine (4.00 mL, 28.8 mmol) in dry THF (27.5 mL) under inert atmosphere and carefully adding *n*-BuLi (13.1 mL, 28.8 mmol) to the solution at 0 °C. LDA was stirred for 20 min at 0 °C and then cooled to −78 °C followed by dropwise addition of *tert*-butyl acetate (3.86 mL, 28.8 mmol) dissolved in dry THF (9.0 mL). The resulting solution was stirred for 20 min, and then the solution of the acyl imidazole 6 was added dropwise at −78 °C and allowed to stir for an additional 45 min. The reaction was quenched by addition of 1 M aqueous solution of HCl (90 mL) at −78 °C, and the resulting mixture was extracted three times with EtOAc (3 × 45 mL), dried over anhydrous MgSO₄, and concentrated by rotatory evaporation to give a thick yellow oil. Finally the crude product was purified by flash column chromatography using a mixture of EtOAc and hexane as the eluent (1:5 to 1:1) to give the title compound as a colorless oil (2.88 g, 72%). *R*_f = 0.37 (EtOAc/hexane, 1:5); ¹H NMR (400 MHz, CDCl₃) δ 7.76 (d, *J* = 7.5, 2H), 7.60 (d, *J* = 7.0, 2H), 7.40 (t, *J* = 7.4, 2H), 7.31 (t, *J* = 7.4, 2H), 5.51 (d, *J* = 8.0, 1H), 4.52–4.39 (m, 3H), 4.21 (t, *J* = 6.7, 1H), 3.4, 3.5 (ABq, *J*_{AB} = 6.9, 2H), 1.96–1.81 (m, 1H), 1.66–1.29 (m, 12H), 0.94 (t, *J* = 7.3, 3H); ¹³C NMR (101 MHz, CDCl₃) δ 202.2, 165.9, 156.0, 143.7, 141.3, 127.6, 127.0, 125.0, 119.9, 66.8, 59.8, 47.4, 47.2, 32.9, 28.2, 27.9, 18.4, 13.7; [α]_D²⁵ +14.3 (*c* = 1.26, CHCl₃); HRMS (ESI) *m/z* [M + Na]⁺ calcd for C₂₆H₃₁O₅NNa 460.2094; found 460.2088.

Methyl (R)-2-(((Trifluoromethyl)sulfonyl)oxy)propanoate (2a). Methyl (R)-lactate (1.62 mL, 16.9 mmol) was dissolved in dry CH₂Cl₂ (68 mL) at 0 °C under argon atmosphere, and triflic anhydride (3.0 mL, 17.8 mmol) was added under stirring followed by slow addition of 2,6-lutidine (2.07 mL, 17.8 mmol). The resulting yellow solution was stirred for 25 min during which it obtained a stronger yellow color. The reaction mixture was concentrated by rotatory evaporation, and the resulting rust-colored residue was dissolved in hexane (508 mL) and cooled in a dry ice bath to ca. −78 °C, thus leading to the precipitation of the lutidinium salt. The precipitate was triturated, filtered off, and washed with hexane, and the combined filtrate was concentrated to give the triflate as a pale liquid (2.64 g, 66%). ¹H NMR (400 MHz, CDCl₃) δ 5.24 (q, *J* = 7.0, 1H), 3.85 (s, 3H), 1.71 (d, *J* = 7.0, 3H); ¹³C NMR (101 MHz, CDCl₃) δ 168.0, 118.6 (q, *J*_{C,F} = 319.8), 80.0, 53.5, 18.2; HRMS (ESI) *m/z* [M + H]⁺ calcd for C₅H₈F₃O₅S 237.0039; found 237.0043.

Methyl (2R,5S)-5-(((9H-Fluoren-9-yl)methoxy)carbonyl)amino)-2-methyl-4-oxooctanoate (7). The protected keto ester 1 (1.84 g, 4.20 mmol) was dissolved in dry THF (16.0 mL) and added to a stirred suspension of NaH (60% in mineral oil, 0.20 g, 5.00 mmol) in dry THF (16.0 mL) at −20 °C. The mixture was stirred for 20 min at −20 °C followed by addition of a solution of the triflate 2a (0.990 g, 4.20 mmol) in dry THF (7.5 mL). The reaction mixture was allowed to warm to room temperature and stirred additionally for 3.5 h, after which the reaction was quenched by addition of a 10% aqueous solution of citric acid (16.0 mL). The resulting mixture was extracted with EtOAc (3 × 80 mL), and the combined organic layer was washed with an aqueous solution of NaHCO₃ and dried over anhydrous MgSO₄. (When the alkylation of 1 was carried out using triflate dissolved in CH₂Cl₂, as has previously been reported to work well,⁴⁰ a thick honey-like crude product with added mass was obtained. TLC analysis revealed that this product contained several unidentified components.) The crude product was purified by flash column chromatography eluting with a mixture of hexanes and EtOAc (5:1 to pure EtOAc) to give the bis-ester as a white precipitate/oil mixture after concentration. The bis-ester 3a (1.77 g, 4.20 mmol) was dissolved in CH₂Cl₂ (21.0 mL), and TFA (3.0 mL) was added. The resulting solution was stirred at room temperature for 24 h and then diluted with CH₂Cl₂ (100 mL) followed by washing with an aqueous solution of NaHCO₃ (2 × 100 mL). The organic layer was dried over anhydrous MgSO₄ and concentrated by rotatory evaporation to give an orange/brownish oil. The crude product was purified by flash column chromatography using a mixture of hexanes and EtOAc (2:1 to pure EtOAc) as the eluent, giving the title compound as a white solid over two steps (1.10 g, 74%, contains trace amount of EtOAc). *R*_f

= 0.31 (hexanes/EtOAc, 2:1); mp = 80 °C; ^1H NMR (400 MHz, CDCl_3) δ = 7.76 (d, J = 7.5, 2H), 7.59 (d, J = 6.1, 2H), 7.40 (t, J = 7.4, 2H), 7.31 (t, J = 7.2, 2H), 5.43 (d, J = 7.1, 1H), 4.45–4.34 (m, 3H), 4.21 (t, J = 6.8, 1H), 3.68 (s, 3H), 3.13–2.91 (m, 2H), 2.65–2.42 (m, 1H), 1.91–1.83 (m, 1H), 1.75–1.47 (m, 1H), 1.45–1.09 (m, 5H), 0.96 (t, J = 7.3, 3H); ^{13}C NMR (101 MHz, CDCl_3) δ 207.4, 176.1, 156.2, 144.0, 141.4, 127.8, 127.2, 125.2, 120.1, 67.0, 59.6, 52.0, 47.3, 43.4, 34.4, 33.7, 18.5, 17.3, 14.0; HRMS (ESI) m/z $[\text{M} + \text{Na}]^+$ calcd for $\text{C}_{23}\text{H}_{29}\text{O}_5\text{NNa}$ 446.1938; found 446.1928.

tert-Butyl (R)-2-(((Trifluoromethyl)sulfonyl)oxy)propanoate (2b). *tert*-Butyl-(*R*)-lactate (3.00 g, 20 mmol) was dissolved in dry CH_2Cl_2 (80 mL), and the reaction mixture was cooled to 0 °C under an argon atmosphere. 2,6-Lutidine (3.49 mL, 30 mmol) was added giving rise to bubble formation, and then triflic anhydride (4.71 mL, 28 mmol) was added over a period of 70 min using a syringe pump, upon which the solution turned purple and then dark yellowish. The reaction mixture was stirred for an additional 1 h at 0 °C and then diluted with petroleum ether 40–60 (100 mL) forming a rusty colored oil. An additional 300 mL of petroleum ether 40–60 was added, and the organic layer was washed with a mixture of 1 M HCl and a saturated aqueous solution of NaCl (1:3, 3 \times 200 mL), dried over MgSO_4 , and concentrated by rotatory evaporation. The crude whiteish liquid was purified by isocratic flash column chromatography using a mixture of CH_2Cl_2 and petroleum ether (1:1) as the eluent, giving the title compound as a colorless liquid (4.97 g, 89%). R_f = 0.79 (CH_2Cl_2 /petroleum ether; 1:1); ^1H NMR (400 MHz, CDCl_3) δ 5.09 (q, J = 7.0, 1H), 1.66 (d, J = 7.0, 3H), 1.51 (s, 9H); ^{13}C NMR (101 MHz, CDCl_3) δ 166.6, 118.5 (q, $J_{\text{C,F}}$ = 319.4 Hz), 84.5, 80.7, 27.9, 18.1; $[\alpha]_{\text{D}}^{25}$ +37.5 (c = 1.29, CHCl_3); HRMS (ESI) m/z $[\text{M} + \text{H}]^+$ calcd for $\text{C}_8\text{H}_{14}\text{F}_3\text{O}_5\text{S}$ 279.0514; found 279.0513.

(2*R*,5*S*)-5-(((9*H*-Fluoren-9-yl)methoxy)carbonyl)amino)-2-methyl-4-oxooctanoic Acid (4). The *tert*-butyl keto ester **1** (2.54 g, 5.80 mmol) was dissolved in dry THF (22.3 mL) and added dropwise at –5 °C to a stirred suspension of NaH (60% in mineral oil, 0.280 g, 6.96 mmol) in dry THF (22.3 mL). The resulting pale yellowish mixture was stirred for 20 min at –5 °C followed by addition of triflate **2b** (1.77 g, 6.38 mmol) dissolved in dry THF (11.2 mL). After 3 h of stirring at room temperature, the reaction mixture was quenched by addition of 1 M HCl (170 mL), extracted with EtOAc (3 \times 110 mL), washed with a saturated aqueous solution of NaCl (335 mL), and finally dried over MgSO_4 . The resulting solution was concentrated by rotatory evaporation to give a honey-like oil, which was dissolved in CH_2Cl_2 (58 mL) and trifluoroacetic acid (8.7 mL). After 24 h of stirring, the dark green solution was concentrated by rotatory evaporation, and the obtained brownish oil was dissolved in dichloromethane (110 mL) and washed with a saturated aqueous solution of NaCl (1 \times 110 mL). The organic layer was dried over MgSO_4 and concentrated by rotatory evaporation to a dark brownish oil, which was purified by flash column chromatography using CH_2Cl_2 and MeOH (97.5:2.5 to 95:5) to give the title compound as a white foam (0.800 g, 34% over three steps). Mp = decomp; R_f = 0.28 (CH_2Cl_2 /MeOH, 95:5); ^1H NMR (400 MHz, CDCl_3) δ 7.76 (d, J = 7.5, 2H), 7.59 (d, J = 6.9, 2H), 7.40 (t, J = 7.4, 2H), 7.31 (t, J = 7.4, 2H), 5.45 (d, J = 7.4, 1H), 4.49–4.27 (m, 3H), 4.21 (t, J = 6.8, 1H), 3.10–2.92 (m, 2H), 2.54 (dd, J = 20.7, 7.1, 1H), 1.95–1.79 (m, 1H), 1.62–1.47 (m, 1H), 1.42–1.11 (m, 5H), 0.94 (t, J = 7.1, 3H); ^{13}C NMR (101 MHz, CDCl_3) δ 207.3, 181.1, 156.2, 144.0, 143.9, 141.5, 127.9, 127.2, 125.2, 120.1, 67.1, 59.5, 47.3, 43.1, 34.4, 33.6, 18.4, 17.1, 13.9; $[\alpha]_{\text{D}}^{25}$ +27.4 (c = 1.01, CHCl_3); HRMS (ESI) m/z $[\text{M} + \text{H}]^+$ calcd for $\text{C}_{24}\text{H}_{28}\text{NO}_5$ 410.1968; found 410.1969.

(R)-2-Hydroxypropanoic Acid (10). To a stirred solution of *D*-alanine (**9**; 0.222 g, 2.50 mmol) in 0.7 M aqueous TFA (4.9 mL) at room temperature was added a solution of sodium nitrite (0.259 g, 3.75 mmol) in milliQ water (2.5 mL) over a period of 3 h using a syringe pump. The reaction mixture was left under stirring for additional 3 h, and NaCl (0.500 g) was added. The aqueous solution was extracted with EtOAc (4 \times 15 mL), the combined organic layers were dried over MgSO_4 , and the solvent was removed to give the title compound as a yellowish oil (0.139 g, 62%). ^1H NMR (400 MHz, D_2O) δ 4.34 (q, J = 7.0, 1H), 1.37 (d, J = 7.0, 3H); ^{13}C NMR (101

MHz, D_2O) δ 181.4, 69.2, 22.1; HRMS (ESI) m/z $[\text{M} + \text{Na}]^+$ calcd for $\text{C}_3\text{H}_6\text{O}_3\text{Na}$ 113.0209; found 113.0204.

Benzyl (R)-2-Hydroxypropanoate (11). (*R*)-Lactic acid (**10**; 50.0 mg, 0.560 mmol) was dissolved in methanol (3.0 mL), and a 20% aqueous solution of Cs_2CO_3 was added until pH 7. The mixture was concentrated by rotatory evaporation, yielding a white precipitate, which was dissolved in DMF (2.0 mL), and benzyl bromide (66 μL , 0.560 mmol) was added under stirring. The resulting mixture was stirred for 6 h at room temperature before it was partitioned between EtOAc (20 mL) and water (20 mL). The aqueous layer was extracted twice more with EtOAc (20 mL), the combined organic layers were dried over anhydrous MgSO_4 , and the solvent was removed *in vacuo* to give the title compound as a colorless liquid/oil containing traces of water (75 mg, 75%). ^1H NMR (400 MHz, CDCl_3) δ 7.42–7.33 (m, 5H), 5.22 (s, 2H), 4.37–4.28 (m, 1H), 2.76 (d, J = 5.3, 1H), 1.44 (d, J = 6.9, 3H); ^{13}C NMR (101 MHz, CDCl_3) δ 175.7, 135.3, 128.8, 128.7, 128.4, 67.5, 67.0, 20.5; HRMS (ESI) m/z $[\text{M} + \text{Na}]^+$ calcd for $\text{C}_{10}\text{H}_{12}\text{O}_3\text{Na}$ 203.0679; found 203.0679.

Benzyl (R)-2-(((Trifluoromethyl)sulfonyl)oxy)propanoate (2c). To a cold solution (0 °C) of the benzyl lactate **11** (0.957 g, 5.32 mmol) in CH_2Cl_2 (21.0 mL) was added triflic anhydride (0.940 mL, 5.59 mmol) followed by slow addition of 2,6-lutidine (0.620 mL, 5.32 mmol) under stirring. After 1 h of stirring, the reaction solution was concentrated by rotatory evaporation, dissolved in hexanes (100 mL), and cooled in a dry ice bath for several minutes, thus leading to the precipitation of the lutidinium salt. The precipitate was filtered off and washed with hexanes, and the combined filtrate was concentrated to give the title compound as a colorless liquid (1.05 g, 63%). The triflate was used in the next step without further purification. ^1H NMR (400 MHz, CDCl_3) δ 7.44–7.27 (m, 5H), 5.32–5.17 (m, 3H), 1.71 (d, J = 7.0, 3H); ^{13}C NMR (101 MHz, CDCl_3) δ 167.4, 134.5, 129.0, 128.9, 128.6, 118.6 (q, $J_{\text{C,F}}$ = 319.8 Hz), 80.1, 68.4, 18.2; HRMS (DART) m/z $[\text{M} + \text{H}_2\text{O}]^+$ calcd for $\text{C}_{11}\text{H}_{13}\text{F}_3\text{O}_6\text{S}$ 330.0385; found 330.0382.

Allyl (S)-4-((tert-Butoxycarbonyl)amino)-3-oxoheptanoate (13). CDI (1.13 g, 6.95 mmol) was added to a stirring solution of Boc-Nva-OH (**12**) (1.44 g, 6.62 mmol) in dry THF (13.5 mL) at room temperature under argon atmosphere. The yellowish solution was stirred for 1 h and used in the next step without further purification. During this hour, a lithium enolate solution was prepared by adding *n*-BuLi (9.28 mL, 2.5 M) to a solution of diisopropylamine (3.28 mL, 23.2 mmol) in dry THF (22.1 mL) at 0 °C. The resulting orange solution was stirred additionally for 10 min and then cooled to –78 °C followed by dropwise addition of allyl acetate (2.50 mL, 23.2 mmol) in dry THF (7.4 mL) and stirring for 15 min. The activated amino acid solution was added dropwise to the lithium enolate solution at –78 °C under inert conditions, and the resulting mixture was stirred for 40 min and then quenched at the same temperature by addition of a 10% aqueous citric acid solution (70 mL). After reaching ambient temperature, the aqueous layer was extracted with EtOAc (3 \times 50 mL), and the combined organic layers were washed with saturated sodium bicarbonate solution (2 \times 100 mL) and a saturated aqueous solution of NaCl (100 mL) and dried over anhydrous MgSO_4 . The solvent was removed to give an orange-colored oily liquid as the crude product, which in turn was purified using a Reveleris automatic flash system using a mixture of hexane and EtOAc as eluents (9:1 to pure EtOAc). The title compound was obtained as a colorless oil (1.66 g, 84%). R_f = 0.63 (hexane/EtOAc, 9:1); ^1H NMR (400 MHz, CDCl_3) δ 5.99–5.83 (m, 1H), 5.38–5.20 (m, 2H), 5.05 (d, J = 7.3, 1H), 4.63 (dd, J = 4.6, 1.2, 2H), 4.39–4.26 (m, 1H), 3.65–3.45 (m, 2H), 1.91–1.70 (m, 1H), 1.64–1.48 (m, 1H), 1.43 (s, 9H), 1.36 (m, 2H), 0.93 (t, J = 7.3, 3H); ^{13}C NMR (101 MHz, CDCl_3) δ 202.4, 166.7, 155.6, 131.6, 119.0, 80.2, 66.2, 59.7, 46.3, 33.1, 28.4, 18.7, 13.9; HRMS (ESI) m/z $[\text{M} + \text{Na}]^+$ calcd for $\text{C}_{15}\text{H}_{25}\text{O}_5\text{NNa}$ 322.1625; found 322.1630.

Benzyl (2*R*,5*S*)-5-((tert-Butoxycarbonyl)amino)-2-methyl-4-oxooctanoate (14). The keto allyl ester **13** (0.871 g, 2.91 mmol) was dissolved in dry THF (11.0 mL) and added dropwise at –20 °C to a stirring suspension of NaH (60% in mineral oil, 0.140 g, 3.49 mmol) in dry THF (11.0 mL). The resulting mixture was stirred for 40 min at –20 °C followed by addition of the triflate **2c** (0.999 g, 3.20 mmol) dissolved in dry THF (6.0 mL). The resulting yellow solution was

allowed to warm to room temperature and was stirred for 3 h before it was quenched with 10% citric acid (11.0 mL). The aqueous layer was extracted with EtOAc (3 × 50 mL), and the combined organic layers were washed with a 10% aqueous NaHCO₃ solution (60 mL) and a saturated aqueous solution of NaCl (60 mL), dried over anhydrous MgSO₄, and concentrated by rotatory evaporation to give a yellow oil. The oil was dissolved in dry THF (22.5 mL) and added slowly under argon to a stirred greenish solution of Pd(OAc)₂ (19.4 mg, 0.086 mmol), PPh₃ (38.2 mg, 0.146 mmol), formic acid (0.211 mL, 5.60 mmol), and triethylamine (1.01 mL, 7.28 mmol) in dry THF (3.0 mL), thus turning the solution yellowish. The mixture was stirred for 24 h at room temperature to give a dark green solution, which was filtered through Celite (500 Å) and concentrated by rotatory evaporation. The crude product was purified by flash column chromatography using a mixture of hexanes and EtOAc as the eluents (9:1 to pure EtOAc) to give the title compound as a yellow oil (0.462 g, 42% over two steps). *R*_f = 0.18 (hexanes/EtOAc, 9:1); ¹H NMR (400 MHz, CDCl₃) δ 7.42–7.28 (m, 5H), 5.15–5.04 (m, 3H), 4.37–4.18 (m, 1H), 3.13–2.91 (m, 2H), 2.62–2.44 (m, 1H), 1.87–1.74 (m, 1H), 1.46–1.26 (m, 12H), 1.20 (d, *J* = 6.7, 3H), 0.97–0.85 (m, 3H); ¹³C NMR (101 MHz, CDCl₃) δ 207.8, 175.5, 155.7, 136.1, 128.6, 128.3, 128.2, 79.8, 66.5, 59.1, 43.3, 34.5, 33.7, 28.4, 18.6, 18.5, 17.3, 13.9; HRMS (ESI) *m/z* [M + Na]⁺ calcd for C₂₁H₃₁O₅NNa 400.2094; found 400.2096.

(2*R*,5*S*)-5-((*tert*-Butoxycarbonyl)amino)-2-methyl-4-oxooctanoic Acid (**8**). To a solution of the keto benzyl ester **14** (31.3 mg, 0.083 mmol) in ethanol (2.3 mL) under inert conditions was added 10% Pd/C (8.9 mg, 0.008 mmol) under stirring at room temperature. The reaction mixture was flushed with H₂ gas and stirred under an H₂ atmosphere (balloon) for 24 h followed by filtration through Celite (500 Å) and concentration *in vacuo* to give the title compound (26 mg, quantitative). ¹H NMR (400 MHz, CDCl₃) δ 5.27–5.01 (m, 1H), 4.39–4.18 (m, 1H), 3.08–2.89 (m, 1H), 2.61–2.45 (m, 1H), 2.24–2.09 (m, 1H), 1.88–1.71 (m, 1H), 1.55–1.27 (m, 12H), 1.23 (d, *J* = 6.8, 3H), 0.92 (t, *J* = 7.2, 3H); ¹³C NMR (101 MHz, CDCl₃) δ 207.9, 180.9, 155.8, 80.0, 59.1, 43.1, 34.3, 33.7, 28.4, 18.6, 17.1, 14.0; HRMS (ESI) *m/z* [M + Na]⁺ calcd for C₁₄H₂₅NO₅Na 310.1625; found 310.1626.

General Procedure for the Synthesis of Peptidomimetics. Rink amide MBHA (100–200 mesh, typically 0.300 g, 0.590 mmol/g loading) was swelled in a synthesis vessel using three-times bed volume of DMF and gentle agitation for ca. 30 min. The solvent was removed by applying vacuum suction, and a solution of 20% piperidine in DMF was added covering the resin, followed by agitation for 5 min and draining by vacuum suction. This procedure was repeated twice more, and the deprotected Rink amide was washed by adding three-times bed volume of DMF and agitating for 1 min and draining of the solvent. The washing procedure was repeated a total of five times. Simultaneously with the washing, a solution of Fmoc-Gln-OH or Fmoc-Glu-EDDnp (4 equiv) and HBTU (3.9 equiv) in a minimum amount of DMF was prepared. To this solution was added DIPEA (8 equiv) followed by thorough mixing and immediate addition to the resin. The reaction mixture was agitated for 1 h, after which the solvent was drained, and the resin was washed five times with DMF and treated with 20% piperidine in DMF as described above. Subsequent coupling of the remaining amino acids using 4 equiv of the Fmoc-protected amino acid, 3.9 equiv of HBTU, and 8 equiv of DIPEA was performed following the same procedure, except for coupling of **4** and **8** where 2 equiv of the dipeptide isosteres were used together with 1.95 equiv of HBTU, and 4 equiv of DIPEA. Boc-deprotection following coupling of **8** was achieved by treating the resin with an initially cold (0 °C) 4 M HCl in dioxane solution under argon atmosphere and agitating at room temperature for 1 h. The resin was washed five times with dioxane and air-dried for 15 min. The dried resin was swelled in DMF with gentle agitation for 30 min and washed 5 times with DMF before coupling of the next amino acid. The deprotection of Fmoc-Asp(O*t*Bu)-OH and Fmoc-Asn(*T*rt)-OH and all subsequent Fmoc-deprotections were carried out using a 20% piperidine in DMF solution containing 0.1 M HOBt in order to suppress aspartimide formation. After the coupling and deprotection

of the last amino acid/fluorophore, the resin was dried by washing five times with DMF, CH₂Cl₂, MeOH, and hexane, respectively, before it was dried by vacuum suction for ca. 30 min. The dry resin was treated in the peptide synthesis vessel with two-times bed volume of a mixture of TFA, TIS, and water (95:2.5:2.5, v/v/v) under gentle agitation for 3 h. The TFA mixture was drained off, and the resin was washed three times with fresh portions of TFA. The combined TFA solution was concentrated by rotatory evaporation, and the obtained residue was precipitated by the addition of cold diethyl ether, followed by trituration. The ether was removed, and the compound was triturated twice more in fresh portions of cold diethyl ether. The crude peptidomimetics were purified by reverse phase HPLC, and the combined fractions were lyophilized to give the desired compounds as fluffy white materials. Peptidomimetics containing the FRET-groups were isolated as fluffy yellow materials.

Keto-D-DY was prepared following the general procedure for SPPS to give the desired compound in 65% purity (UV 220 nm). HRMS (ESI) *m/z* [M + H]⁺ calcd for C₃₉H₆₀N₉O₁₄ 878.4254; found 878.4247.

Keto-D-DY_{FRET} was prepared following the general procedure for SPPS to give the desired compound in >92% purity (UV 220 nm). HRMS (ESI) *m/z* [M + H]⁺ calcd for C₅₄H₇₂N₁₃O₁₉ 1206.5062; found 1206.5044.

Keto-N-ER was prepared following the general procedure for SPPS to give the desired compound in >95% purity (UV 220 nm). HRMS (ESI) *m/z* [M + H]⁺ calcd for C₃₇H₆₆N₁₃O₁₂ 884.4948; found 884.4932.

Keto-N-ER_{FRET} was prepared following the general procedure for SPPS to give the desired compound in >95% purity (UV 220 nm). HRMS (ESI) *m/z* [M + H]⁺ calcd for C₅₂H₇₈N₁₇O₁₇ 1212.5756; found 1212.5742.

Keto-S-ER_{FRET} was prepared following the general procedure for SPPS to give the desired compound in >93% purity. HRMS (ESI) *m/z* [M + H]⁺ calcd for C₅₁H₇₇N₁₆O₁₇ 1185.5653; found 1185.5723.

Biological Studies. Enzyme Assays. The purified enzymes PR3 and HNE were obtained from Athens Research and Technology Inc. (Athens, Georgia, USA). The enzymatic activity of free PR3 and HNE was measured in triplicate in 50 mM HEPES, 750 mM NaCl, supplemented with 0.05% Igepal CA 630 (v/v) at pH 7.4. In order to quantify the effect of the ketomethyls and other inhibitors on PR3 and HNE activities, we assayed the cleavage of the substrate Abz-Val-Ala-Asn-nVal-Ala-Glu-Tyr-Gln-EDDnp (N-EY_{FRET}). We incubated purified PR3 (0.5 nM) with 6 μM of the inhibitors listed in Table 1 for 30 min at room temperature. The same protocol was used for PMSF and α1-PI, while PR3 alone was used as a control. The reaction was started by adding 5 μM of the substrate N-EY_{FRET} to the reaction buffer (20 μL total volume) in 384-well black nonbinding plates (Greiner bio-one #784900). The progress of the hydrolytic reaction was determined by measuring the fluorescence for 30 min at 37 °C with an EnSpire multimode plate reader (PerkinElmer) with 320 and 420 nm excitation and emission wavelengths, respectively, at 37 °C. Similarly, 0.5 nM HNE was incubated for 30 min at room temperature with 6 μM of the above-mentioned inhibitors. Unlike for PR3, the reaction was initiated by adding 5 μM substrate MeOSuc-AAPV-AMC (Santa Cruz Biotechnology, Heidelberg, Germany, Cat. No. sc-201163). The progress of the reaction was monitored as mentioned above but by using excitation wavelength of 355 nM and emission wavelength of 460 nM at 37 °C.

Determination of IC₅₀ Values. We determined the IC₅₀ values for the peptidic inhibitors keto-D-DY_{FRET} and keto-N-ER_{FRET} as well as for two known serine protease inhibitors, PMSF and AIPI. Briefly, 0.5 nM PR3 was incubated for 30 min with 5 μM FRET substrate (D-DY_{FRET}) in the presence of inhibitor concentrations ranging from 0.015 to 100 μM in a 60 μL total volume at 37 °C. The reaction was stopped by addition of 5 μL of 10% TFA and incubation on ice for 10 min. This was followed by centrifugation at 13000g for 10 min at 4 °C. The supernatant was then transferred to HPLC vials sealed with silicon septum and caps. These samples were analyzed to determine hydrolysis products by reverse-phase HPLC using a Shimadzu Prominence instrument fitted with a Machery-Nagel C18 HD column.

Samples were eluted using water/acetonitrile/TFA (0.01% TFA) mobile phase gradients for 55 min. The percentage of enzyme activity was calculated from relative areas under the curve of the (uncleaved) substrate peak. Each experiment was repeated once yielding two independent measures of the activity for each concentration of inhibitor. The dose–response curves are provided as Supporting Information. The IC_{50} values were determined by plotting the logarithm of the concentration of inhibitors with respect to the normalized response using GraphPad Prism. We then perform a nonlinear fit using a standard slope (Hill slope = -1). The 95% confidence interval for each determined IC_{50} value is reported in Table 3.

Inhibition Mechanism. To determine whether the inhibition proceeds using a competitive mechanism, we incubated 0.2 nM PR3 with eight different concentrations (0–6 μ M) of the substrate Abz-Val-Ala-Asp-nVal-Ala-Asp-Tyr-Gln-EDDnp (D-DY_{FRET}) and concentrations of 0–4 μ M of the inhibitor keto-D-DY_{FRET} to the reaction buffer (20 μ L total volume) in 384-well black nonbinding plates in a single experimental setup. The reaction was followed using the EnSpire multimode plate reader as described above. The reaction velocities were calculated after blank correction; the substrate titration and the double reciprocal plots were subsequently generated using GraphPad Prism v.5. Further, to check the reversibility of the inhibition mechanism, we performed a rapid dilution assay. An enzyme concentration of 50 nM, that is, 100-fold larger than that used for the activity assay, was incubated for 30 min with inhibitor keto-D-DY_{FRET} at a concentration of 19 μ M corresponding to about 10 times its measured IC_{50} value. This mixture was then rapidly diluted 100-fold into the reaction mixture containing 8 μ M of the corresponding FRET substrate, that is, D-DY_{FRET} (20 μ L total reaction volume in 384-well plates). The experiment was run in triplicate. The progress of the reaction was monitored using a plate reader as described above.

■ ASSOCIATED CONTENT

● Supporting Information

Free energy decomposition from molecular dynamics simulations, curves with error bars from the rapid dilution experiment, independent IC_{50} measurements, summaries of 1H and ^{13}C signals, and full structural assignment for keto-D-DY_{FRET}, keto-N-ER_{FRET}, and keto-S-ER_{FRET}. This material is available free of charge via the Internet at <http://pubs.acs.org>.

■ AUTHOR INFORMATION

Corresponding Authors

*N.R. Tel: (+47) 55584040. E-mail: nathalie.reuter@mbi.uib.no.

*B.E.H. Tel: (+47) 55583468. E-mail: bengt-erik.haug@farm.uib.no.

Present Address

¹C.G.: Institute of Biomedical Sciences, Academia Sinica, Taipei 115, Taiwan.

Author Contributions

[#]A.B. and S.N. contributed equally.

The manuscript was written through contributions of all authors. All authors have given approval to the final version of the manuscript.

Notes

The authors declare no competing financial interest.

■ ACKNOWLEDGMENTS

This work was supported by grants from the Bergen Research Foundation and the Meltzer foundation to N.R., A.-S.S., C.G., and S.N. and by a grant from BTO-Visjon vest to N.R. and B.E.H. Parallab and NOTUR are thankfully acknowledged for provision of CPU time.

■ ABBREVIATIONS

A1AT, α -1 antitrypsin; α 1PI, α -1 protease inhibitor; Abz, 2-aminobenzoic acid; All, allyl; AMC, 7-amino-4-methylcoumarin; ANCA, antineutrophil cytoplasmic antibody; CDI, 1,1'-carbonyldiimidazole; COPD, chronic obstructive pulmonary disease; EDDnp, *N*-(2,4-dinitrophenyl)-ethylenediamine; GPA, granulomatosis with polyangiitis; HNE, human neutrophil elastase; HOBt, *N*-hydroxybenzotriazole; MD, molecular dynamics; MeOSuc, *N*-methoxysuccinyl; MM/PBSA, molecular mechanics/Poisson–Boltzmann surface area; NSP, neutrophil serine protease; nV, norvaline; Pbf, 2,2,4,6,7-pentamethyl-dihydrobenzofuran-5-sulfonyl; PMN, polymorphonuclear neutrophils; PMSF, phenylmethanesulfonyl fluoride; PR3, proteinase 3; SPPS, solid phase peptide synthesis

■ REFERENCES

- (1) Nathan, C. Neutrophils and immunity: Challenges and opportunities. *Nat. Rev. Immunol.* **2006**, *6*, 173–182.
- (2) Amulic, B.; Cazalet, C.; Hayes, G. L.; Metzler, K. D.; Zychlinsky, A. Neutrophil function: From mechanisms to disease. *Annu. Rev. Immunol.* **2012**, *30*, 459–489.
- (3) Pham, C. T. N. Neutrophil serine proteases: specific regulators of inflammation. *Nat. Rev. Immunol.* **2006**, *6*, 541–550.
- (4) Pham, C. T. N. Neutrophil serine proteases fine-tune the inflammatory response. *Int. J. Biochem. Cell Biol.* **2008**, *40*, 1317–1333.
- (5) Groutas, W. C.; Dou, D.; Alliston, K. R. Neutrophil elastase inhibitors. *Expert Opin. Ther. Pat.* **2011**, *21*, 339–354.
- (6) Malech, H. L.; Gallin, J. I. Current concepts: Immunology. Neutrophils in human diseases. *New Engl. J. Med.* **1987**, *317*, 687–694.
- (7) Voynow, J. A.; Fischer, B. M.; Zheng, S. Proteases and cystic fibrosis. *Int. J. Biochem. Cell Biol.* **2008**, *40*, 1238–1245.
- (8) Witko-Sarsat, V.; Lesavre, P.; Lopez, S.; Bessou, G.; Hieblot, C.; Prum, B.; Noel, L. H.; Guillevin, L.; Ravaud, P.; Sermet-Gaudelus, I.; Timsit, J.; Grunfeld, J. P.; Halbwachs-Mecarelli, L. A large subset of neutrophils expressing membrane proteinase 3 is a risk factor for vasculitis and rheumatoid arthritis. *J. Am. Soc. Nephrol.* **1999**, *10*, 1224–1233.
- (9) Lucas, S. D.; Costa, E.; Guedes, R. C.; Moreira, R. Targeting COPD: Advances on low-molecular-weight inhibitors of human neutrophil elastase. *Med. Res. Rev.* **2013**, *33*, E73–E101.
- (10) Lyons, P. A.; Rayner, T. F.; Trivedi, S.; Holle, J. U.; Watts, R. A.; Jayne, D. R. W.; Baslund, B.; Brenchley, P.; Bruchfeld, A.; Chaudhry, A. N.; Tervaert, J. W. C.; Deloukas, P.; Feighery, C.; Gross, W. L.; Guillevin, L.; Gunnarsson, I.; Harper, L.; Hruskova, Z.; Little, M. A.; Martorana, D.; Neumann, T.; Ohlsson, S.; Padmanabhan, S.; Pusey, C. D.; Salama, A. D.; Sanders, J. S. F.; Savage, C. O.; Segelmark, M.; Stegeman, C. A.; Tesar, V.; Vaglio, A.; Wieczorek, S.; Wilde, B.; Zwerina, J.; Rees, A. J.; Clayton, D. G.; Smith, K. G. C. Genetically distinct subsets within ANCA-associated vasculitis. *New Engl. J. Med.* **2012**, *367*, 214–223.
- (11) Korkmaz, B.; Lesner, A.; Letast, S.; Mahdi, Y. K.; Jourdan, M. L.; Dallet-Choisy, S.; Marchand-Adam, S.; Kellenberger, C.; Viaud-Massuard, M. C.; Jenne, D. E.; Gauthier, F. Neutrophil proteinase 3 and dipeptidyl peptidase I (cathepsin C) as pharmacological targets in granulomatosis with polyangiitis (Wegener granulomatosis). *Semin. Immunopathol.* **2013**, *35*, 411–421.
- (12) Sinden, N. J.; Stockley, R. A. Proteinase 3 activity in sputum from subjects with alpha-1-antitrypsin deficiency and COPD. *Eur. Respir. J.* **2013**, *41*, 1042–1050.
- (13) Hajjar, E.; Broemstrup, T.; Kantari, C.; Witko-Sarsat, V.; Reuter, N. Structures of human proteinase 3 and neutrophil elastase—so similar yet so different. *FEBS J.* **2010**, *277*, 2238–2254.
- (14) Schechter, I.; Berger, A. On the size of the active site in proteases. I. Papain. *Biochem. Biophys. Res. Commun.* **1967**, *27*, 157–162.
- (15) S_n , ..., S_2 , S_1 , S_1' , S_2' , ..., S_n' for the recognition sites on the enzyme and P_n , ..., P_2 , P_1 , P_1' , P_2' , ..., P_n' for the corresponding

amino acids of the peptide, where the P1–P1' bond is the bond that is hydrolyzed by the protease.

(16) Hajjar, E.; Korkmaz, B.; Gauthier, F.; Brandsdal, B. O.; Witko-Sarsat, V.; Reuter, N. Inspection of the binding sites of proteinase 3 for the design of a highly specific substrate. *J. Med. Chem.* **2006**, *49*, 1248–1260.

(17) Korkmaz, B.; Hajjar, E.; Kalupov, T.; Reuter, N.; Brillard-Bourdet, M.; Moreau, T.; Juliano, L.; Gauthier, F. Influence of charge distribution at the active site surface on the substrate specificity of human neutrophil protease 3 and elastase. A kinetic and molecular modeling analysis. *J. Biol. Chem.* **2007**, *282*, 1989–1997.

(18) Wysocka, M.; Lesner, A.; Gruba, N.; Korkmaz, B.; Gauthier, F.; Kitamatsu, M.; Legowska, A.; Rolka, K. Three wavelength substrate system of neutrophil serine proteinases. *Anal. Chem.* **2012**, *84*, 7241–7248.

(19) Wysocka, M.; Lesner, A.; Popow, J.; Legowska, M.; Rolka, K. Pegylated fluorescent peptides as substrates of proteolytic enzymes. *Protein Pept. Lett.* **2012**, *19*, 1237–1244.

(20) Chagas, J. R.; Juliano, L.; Prado, E. S. Intramolecularly quenched fluorogenic tetrapeptide substrates for tissue and plasma kallikreins. *Anal. Biochem.* **1991**, *192*, 419–425.

(21) Korkmaz, B.; Moreau, T.; Gauthier, F. Neutrophil elastase, proteinase 3 and cathepsin G: Physicochemical properties, activity and physiopathological functions. *Biochimie* **2008**, *90*, 227–242.

(22) Korkmaz, B.; Attucci, S.; Moreau, T.; Godat, E.; Juliano, L.; Gauthier, F. Design and use of highly specific substrates of neutrophil elastase and proteinase 3. *Am. J. Respir. Cell Mol. Biol.* **2004**, *30*, 801–807.

(23) Narawane, S.; Budnjo, A.; Grauffel, C.; Haug, B. E.; Reuter, N. In silico design, synthesis, and assays of specific substrates for proteinase 3: Influence of fluorogenic and charged groups. *J. Med. Chem.* **2014**, *57*, 1111–1115.

(24) Popow-Stellmaszyk, J.; Wysocka, M.; Lesner, A.; Korkmaz, B.; Rolka, K. A new proteinase 3 substrate with improved selectivity over human neutrophil elastase. *Anal. Biochem.* **2013**, *442*, 75–82.

(25) Kasperkiewicz, P.; Poreba, M.; Snipas, S. J.; Parker, H.; Winterbourn, C. C.; Salvesen, G. S.; Drag, M. Design of ultrasensitive probes for human neutrophil elastase through hybrid combinatorial substrate library profiling. *Proc. Natl. Acad. Sci. U.S.A.* **2014**, *111*, 2518–2523.

(26) Nakayama, Y.; Odagaki, Y.; Fujita, S.; Matsuoka, S.; Hamanaka, N.; Nakai, H.; Toda, M. Clarification of mechanism of human sputum elastase inhibition by a new inhibitor, ONO-5046, using electrospray ionization mass spectrometry. *Bioorg. Med. Chem. Lett.* **2002**, *12*, 2349–2353.

(27) Stockley, R.; De Soyza, A.; Gunawardena, K.; Perrett, J.; Forsman-Semb, K.; Entwistle, N.; Snell, N. Phase II study of a neutrophil elastase inhibitor (AZD9668) in patients with bronchiectasis. *Respir. Med.* **2013**, *107*, 524–533.

(28) Iwata, K.; Doi, A.; Ohji, G.; Oka, H.; Oba, Y.; Takimoto, K.; Igarashi, W.; Gremillion, D. H.; Shimada, T. Effect of neutrophil elastase inhibitor (sivelestat sodium) in the treatment of acute lung injury (ALI) and acute respiratory distress syndrome (ARDS): A systematic review and meta-analysis. *Int. Med.* **2010**, *49*, 2423–2432.

(29) Kawabata, K.; Suzuki, M.; Sugitani, M.; Imaki, K.; Toda, M.; Miyamoto, T. ONO-5046, a novel inhibitor of human neutrophil elastase. *Biochem. Biophys. Res. Commun.* **1991**, *177*, 814–820.

(30) Crocetti, L.; Schepetkin, I. A.; Cilibrizzi, A.; Graziano, A.; Vergelli, C.; Giomi, D.; Khlebnikov, A. I.; Quinn, M. T.; Giovannoni, M. P. Optimization of N-benzoylindazole derivatives as inhibitors of human neutrophil elastase. *J. Med. Chem.* **2013**, *56*, 6259–6272.

(31) Lucas, S. D.; Gonçalves, L. M.; Carvalho, L. A. R.; Correia, H. F.; Da Costa, E. M. R.; Guedes, R. A.; Moreira, R.; Guedes, R. C. Optimization of O₃-acyl kojic acid derivatives as potent and selective human neutrophil elastase inhibitors. *J. Med. Chem.* **2013**, *56*, 9802–9806.

(32) Groutas, W. C.; Hoidal, J. R.; Brubaker, M. J.; Stanga, M. A.; Venkataraman, R.; Gray, B. H.; Rao, N. V. Inhibitors of human leukocyte proteinase-3. *J. Med. Chem.* **1990**, *33*, 1085–1087.

(33) Groutas, W. C.; Epp, J. B.; Venkataraman, R.; Kuang, R.; Truong, T. M.; McClenahan, J. J.; Prakash, O. Design, synthesis, and in vitro inhibitory activity toward human leukocyte elastase, cathepsin G, and proteinase 3 of saccharin-derived sulfones and congeners. *Bioorg. Med. Chem.* **1996**, *4*, 1393–1400.

(34) Groutas, W. C.; Kuang, R.; Ruan, S.; Epp, J. B.; Venkataraman, R.; Truong, T. M. Potent and specific inhibition of human leukocyte elastase, cathepsin G and proteinase 3 by sulfone derivatives employing the 1,2,5-thiadiazolidin-3-one 1,1 dioxide scaffold. *Bioorg. Med. Chem.* **1998**, *6*, 661–671.

(35) EpINETTE, C.; Croix, C.; Jaquillard, L.; Marchand-Adam, S.; Kellenberger, C.; Lalmanach, G.; Cadene, M.; Viaud-Massuard, M. C.; Gauthier, F.; Korkmaz, B. A selective reversible azapeptide inhibitor of human neutrophil proteinase 3 derived from a high affinity FRET substrate. *Biochem. Pharmacol.* **2012**, *83*, 788–796.

(36) Cheng, L.; Goodwin, C. A.; Schully, M. F.; Kakkar, V. V.; Claeson, G. Synthesis and biological activity of ketomethylene pseudopeptide analogues as thrombin inhibitors. *J. Med. Chem.* **1992**, *35*, 3364–3369.

(37) Singh, J.; Petter, R. C.; Baillie, T. A.; Whitty, A. The resurgence of covalent drugs. *Nat. Rev. Drug Discovery* **2011**, *10*, 307–317.

(38) Noe, M. C.; Gilbert, A. M. Targeted covalent enzyme inhibitors. *Annu. Rep. Med. Chem.* **2012**, *47*, 413–439.

(39) Hoffman, R. V.; Tao, J. A simple, stereoselective synthesis of ketomethylene dipeptide isosteres. *Tetrahedron* **1997**, *53*, 7119–7126.

(40) Hoffman, R. V.; Tao, J. Synthesis of Cbz-protected ketomethylene dipeptide isosteres. *Method. Mol. Med.* **1999**, *23*, 103–124.

(41) Di Gioia, M. L.; Leggio, A.; Le Pera, A.; Liguori, A.; Perri, F.; Siciliano, C. Alternative and chemoselective deprotection of the α -amino and carboxy functions of N-Fmoc-amino acid and N-Fmoc-dipeptide methyl esters by modulation of the molar ratio in the AlCl₃/N,N-dimethylaniline reagent system. *Eur. J. Org. Chem.* **2004**, *2004*, 4437–4441.

(42) Nicolaou, K. C.; Estrada, A. A.; Zak, M.; Lee, S. H.; Safina, B. S. A mild and selective method for the hydrolysis of esters with trimethyltin hydroxide. *Angew. Chem., Int. Ed.* **2005**, *44*, 1378–1382.

(43) Mittag, T.; Otzen, D. E.; Nielsen, N. C.; Skrydstrup, T. Synthesis of a ketomethylene isostere of the fibrillating peptide SNNFGAILSS. *J. Org. Chem.* **2009**, *74*, 7955–7957.

(44) Gonzalez-Muniz, R.; Garcia-Lopez, M. T.; Gomez-Monterrey, I.; Herranz, R.; Jimeno, M. L.; Suarez-Gea, M. L.; Johansen, N. L.; Madsen, K.; Thogersen, H.; Suzdak, P. Ketomethylene and (cyanomethylene)amino pseudopeptide analogs of the C-terminal hexapeptide of neurotensin. *J. Med. Chem.* **1995**, *38*, 1015–1021.

(45) Våbenø, J.; Nielsen, C. U.; Ingebrigtsen, T.; Lejon, T.; Steffansen, B.; Luthman, K. Dipeptidomimetic ketomethylene isosteres as pro-moieties for drug transport via the human intestinal di-/tripeptide transporter hPEPT1: Design, synthesis, stability, and biological investigations. *J. Med. Chem.* **2004**, *47*, 4755–4765.

(46) Martinez, J.; Bodanszky, M. Side reactions in peptide synthesis. *Int. J. Pept. Protein Res.* **1978**, *12*, 277–283.

(47) Subirós-Funosas, R.; El-Faham, A.; Albericio, F. Aspartimide formation in peptide chemistry: Occurrence, prevention strategies and the role of N-hydroxylamines. *Tetrahedron* **2011**, *67*, 8595–8606.

(48) Hoffman, R. V.; Maslough, N.; Cervantes-Lee, F. Highly stereoselective syntheses of syn- and anti-1,2-amino alcohols. *J. Org. Chem.* **2001**, *67*, 1045–1056.

(49) Han, G.; Tamaki, M.; Hruby, V. J. Fast, efficient and selective deprotection of the tert-butoxycarbonyl (Boc) group using HCl/dioxane (4 M). *J. Pept. Res.* **2001**, *58*, 338–341.

(50) Schepetkin, I. A.; Khlebnikov, A. I.; Quinn, M. T. N-benzoylpyrazoles are novel small-molecule inhibitors of human neutrophil elastase. *J. Med. Chem.* **2007**, *50*, 4928–4938.

(51) Copeland, R. A. *Evaluation of Enzyme Inhibitors in Drug Discovery: A Guide for Medicinal Chemists and Pharmacologists*; Wiley: Hoboken, N.J., USA, 2005.

(52) Campbell, E. J.; Campbell, M. A.; Owen, C. A. Bioactive proteinase 3 on the cell surface of human neutrophils: Quantification,

catalytic activity, and susceptibility to inhibition. *J. Immunol.* **2000**, *165*, 3366–3374.

(53) Copeland, R. A.; Lombardo, D.; Giannaras, J.; Decicco, C. P. Estimating K_i values for tight-binding inhibitors from dose-response plots. *Bioorg. Med. Chem. Lett.* **1995**, *5*, 1947–1952.

(54) Cer, R. Z.; Mudunuri, U.; Stephens, R.; Lebeda, F. J. IC_{50} -to- K_i : a web-based tool for converting IC_{50} to K_i values for inhibitors of enzyme activity and ligand binding. *Nucleic Acids Res.* **2009**, *37*, W441–W445.

(55) Hedstrom, L. Serine protease mechanism and specificity. *Chem. Rev.* **2002**, *102*, 4501–4524.

(56) MacKerell, A. D.; Bashford, D.; Bellott, M.; Dunbrack, R. L.; Evanseck, J. D.; Field, M. J.; Fischer, S.; Gao, J.; Guo, H.; Ha, S.; Joseph-McCarthy, D.; Kuchnir, L.; Kuczera, K.; Lau, F. T. K.; Mattos, C.; Michnick, S.; Ngo, T.; Nguyen, D. T.; Prodhom, B.; Reiher, W. E.; Roux, B.; Schlenkrich, M.; Smith, J. C.; Stote, R.; Straub, J.; Watanabe, M.; Wiórkiewicz-Kuczera, J.; Yin, D.; Karplus, M. All-atom empirical potential for molecular modeling and dynamics studies of proteins. *J. Phys. Chem. B* **1998**, *102*, 3586–3616.

(57) Mackerell, A. D.; Feig, M.; Brooks, C. L. Extending the treatment of backbone energetics in protein force fields: Limitations of gas-phase quantum mechanics in reproducing protein conformational distributions in molecular dynamics simulations. *J. Comput. Chem.* **2004**, *25*, 1400–1415.

(58) Brooks, B. R.; Brooks, C. L., 3rd; Mackerell, A. D., Jr.; Nilsson, L.; Petrella, R. J.; Roux, B.; Won, Y.; Archontis, G.; Bartels, C.; Boresch, S.; Caffisch, A.; Caves, L.; Cui, Q.; Dinner, A. R.; Feig, M.; Fischer, S.; Gao, J.; Hodoscek, M.; Im, W.; Kuczera, K.; Lazaridis, T.; Ma, J.; Ovchinnikov, V.; Paci, E.; Pastor, R. W.; Post, C. B.; Pu, J. Z.; Schaefer, M.; Tidor, B.; Venable, R. M.; Woodcock, H. L.; Wu, X.; Yang, W.; York, D. M.; Karplus, M. CHARMM: The biomolecular simulation program. *J. Comput. Chem.* **2009**, *30*, 1545–1614.

(59) Phillips, J. C.; Braun, R.; Wang, W.; Gumbart, J.; Tajkhorshid, E.; Villa, E.; Chipot, C.; Skeel, R. D.; Kale, L.; Schulten, K. Scalable molecular dynamics with NAMD. *J. Comput. Chem.* **2005**, *26*, 1781–1802.

(60) Lafont, V.; Schaefer, M.; Stote, R.; Altschuh, D.; Dejaegere, A. Protein-protein recognition and interaction hot spots in an antigen-antibody complex: Free energy decomposition identifies efficient amino acids. *Proteins* **2007**, *67*, 418–434.

(61) Davis, M. E.; Madura, J. D.; Luty, B. A.; McCammon, J. A. Electrostatics and diffusion of molecules in solution: Simulations with the University of Houston Brownian dynamics program. *Comput. Phys. Commun.* **1991**, *62*, 187–197.